Suppression of chaotic bursting synchronization in clustered scale-free networks by an external feedback signal

Cite as: Chaos **31**, 083128 (2021); doi: 10.1063/5.0056672
Submitted: 12 May 2021 · Accepted: 2 August 2021 ·
Published Online: 23 August 2021

Adriane S. Reis,[1,a)] Eduardo L. Brugnago,[2] Iberê L. Caldas,[3] Antonio M. Batista,[4] Kelly C. Iarosz,[5] Fabiano A. S. Ferrari,[6,7] and Ricardo L. Viana[2]

AFFILIATIONS

[1]Physics Institute, University of São Paulo, 05508-090 São Paulo, SP, Brazil
[2]Physics Department, Federal University of Paraná, 81531-980 Curitiba, PR, Brazil
[3]Physics Institute, University of São Paulo, 81531-980 São Paulo, SP, Brazil
[4]Department of Mathematics and Statistics, State University of Ponta Grossa, 84030-900 Ponta Grossa, PR, Brazil
[5]Faculty of Telêmaco Borba, 84266-010 Telêmaco Borba, PR, Brazil
[6]Institute of Engineering, Science and Technology, Federal University of the Valleys of Jequitinhonha and Mucuri, 39803-371 Janaúba, MG, Brazil
[7]Graduate Program in Computational Modeling and Systems, University of Montes Claros, Montes Claros 39401-089, MG, Brazil

[a)]**Author to whom correspondence should be addressed:** asr.anne@gmail.com

ABSTRACT

Oscillatory activities in the brain, detected by electroencephalograms, have identified synchronization patterns. These synchronized activities in neurons are related to cognitive processes. Additionally, experimental research studies on neuronal rhythms have shown synchronous oscillations in brain disorders. Mathematical modeling of networks has been used to mimic these neuronal synchronizations. Actually, networks with scale-free properties were identified in some regions of the cortex. In this work, to investigate these brain synchronizations, we focus on neuronal synchronization in a network with coupled scale-free networks. The networks are connected according to a topological organization in the structural cortical regions of the human brain. The neuronal dynamic is given by the Rulkov model, which is a two-dimensional iterated map. The Rulkov neuron can generate quiescence, tonic spiking, and bursting. Depending on the parameters, we identify synchronous behavior among the neurons in the clustered networks. In this work, we aim to suppress the neuronal burst synchronization by the application of an external perturbation as a function of the mean-field of membrane potential. We found that the method we used to suppress synchronization presents better results when compared to the time-delayed feedback method when applied to the same model of the neuronal network.

The brain is a complex structure that controls the functioning of the body. The outermost layer of the brain is the cortex, which is composed of billions of neurons. Connections occur among neurons within the same region and also among neurons in different brain regions. Network models of coupled neurons have been developed to mimic neuronal activities in the brain, for instance, synchronous behavior. Neuronal synchronization is related to many different cognitive functions. It can also be associated with seizures in epilepsy and tremor activity in Parkinson's disease. Due to these facts, studies about synchronous activities are relevant for understanding various processes that arise in the brain. In this work, we build scale-free networks coupled according to a structural cortical network. Depending on the parameters, the neurons can exhibit synchronous behavior. Considering an external perturbation that behaves as a selector switch, we propose a signal as a function of the mean-field of membrane potential variance to suppress synchronization. We show that this perturbation can suppress or considerably reduce network synchronization. By using this method, we obtain better results for suppression of the neuronal network than when using perturbation like the time-delayed feedback method.

I. INTRODUCTION

Networks have been used to describe the behavior of complex dynamical systems, such as electric power grid,[1] World

Wide Web,[2] and metabolic reactions.[3] In neuroscience, networks have been considered to analyze and model neurobiological systems.[4] The neuronal networks are composed of neuron models coupled using different topologies, for instance, random,[5] small-world,[6] and scale-free.[7,8]

Scale-free networks are characterized by a fraction of nodes with a degree that follows a power law.[9] Barabási and Albert[10] demonstrated that a scale-free network can be generated by the addition of new nodes that are attached preferentially to well-connected nodes. Eguíluz *et al.*[11] reported brain functional networks, in which the probability of finding a link as a function of distance and distribution of functional connections are both scale-free. Neuronal networks with scale-free topology can mimic much different neuronal behavior observed in the brain. Lameu *et al.*[12] studied the synchronization of neuronal bursting activities in a clustered scale-free network.

Synchronization plays a crucial role in the brain during different tasks.[13] Neurons spiking in synchrony were identified in the neocortex during sleep and wakefulness.[14] Knoblich *et al.*[15] found synchronous behavior in a mouse primary visual cortex. However, neuronal synchrony in the brain can be associated with disorders.[16] Lehnertz *et al.*[17] reported synchronization in human epileptic brain networks from analyses of electromagnetic signals. Parkinson's disease has been related to synchronous oscillatory dynamics, particularly, in the beta frequency band.[18] Due to this fact, studies about methods to suppress synchronization are important to control undesired rhythms that emerge in brain diseases.

In this work, we construct a network composed of coupled subnetworks with scale-free topology. The subnetworks are connected according to the structural network of the human brain reported by Lo et al.[19] They used diffusion tensor image tractography to build human brain networks. In our network, the local neuronal dynamic is given by the model introduced by Rulkov.[20] The Rulkov neuron is a two-dimensional map that mimics some neuronal behaviors, such as tonic spiking, resting, and chaotic bursts. Coupled Rulkov neurons have been utilized to carry out research about synchronization[21] and brain plasticity.[22] Recently, Reis *et al.*[23] showed the existence of bursting synchronization in neuronal assemblies of scale-free networks based on a human connectivity matrix.[19]

We focus on the suppression of neuronal burst synchronous behavior in clustered scale-free networks by means of external perturbation. Also so, we propose to use a signal as a function of the mean-field of membrane potential variance to suppress neuronal synchronization. Our results show that synchronization can be suppressed by an external signal that acts like a selector switch.

This article is organized as follows. We introduce the network construction in Sec. II. In Secs. III and IV, we show the neuronal network dynamic and the methods used to calculate neuronal synchronization and suppression, respectively. Sections V and VI bring the results and a brief discussion. We draw our conclusions in the last section.

II. NETWORK CONSTRUCTION

The cortex is the outer layer of the brain and is divided into two hemispheres. It is involved in many different functions, such as movement control[24] and learning.[25] The areas in the cortex are organized into an architecture of neuronal networks.[26]

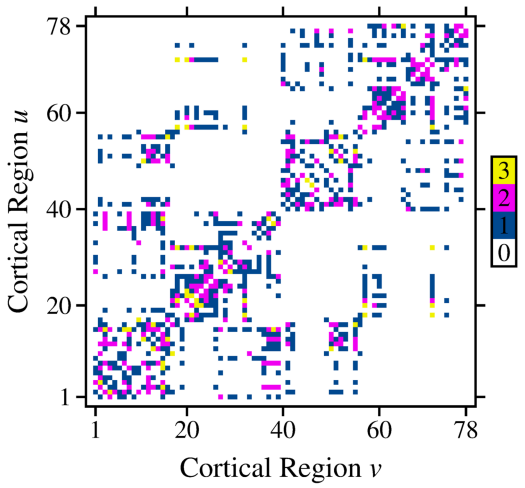

FIG. 1. Representation of the connectivity matrix for healthy humans, divided into 78 cortical regions. Weights are assigned as follow: 0 (white), 1 (blue), 2 (magenta), and 3 (yellow). These weights indicate the lack of connection (or not identified), sparse, intermediate, and dense connections, respectively.

Given the neuronal architecture connections, we build a network with coupled subnetworks, in which the subnetworks have scale-free properties and are coupled using a weighted connection matrix related to the cortical brain structure obtained by Lo *et al.*[19] The structural connection matrix with 78 elements is illustrated in Fig. 1, where the weights are separated into 0 for no connections (white), 1 for low density of connections (blue), 2 for intermediate density of connections (magenta), and 3 for high density of connections (yellow). In our model of coupled scale-free networks, we consider 50, 100, and 150 random connections for the weights 1, 2, and 3, respectively.

For a better understanding of the coupled subnetwork model, we represent a simplified structure of this construction in Fig. 2. On the left side of Fig. 2, each circumference represents a cortical region (subnetwork) coupled through chemical connections (dashed green arrows). As the weighted matrix was divided into 78 cortical regions, we created the same number of subnetworks connected to each other, according to the weight of the matrix. We built the cortical regions as subnetworks composed of 200 neurons in a scale-free network topology,[23] as illustrated on the right side of Fig. 2.

Just as corticocortical connections, all connections made within each subnetwork (blue or gray arrows) are chemical. The growth method for scale-free networks used is in accordance with the Barabási–Albert algorithm.[10,27] The obtained network topology presents the main hub (red circle highlighted in Fig. 2), that is, it is the vertex that presents the majority of connections, and one or more secondary hubs (magenta circle), whose number of links is much larger than in most vertices and less than in the main hub.

Each new neuron added to the network is linked twice: once as a pre-synaptic and then as a post-synaptic. So that, every vertex of

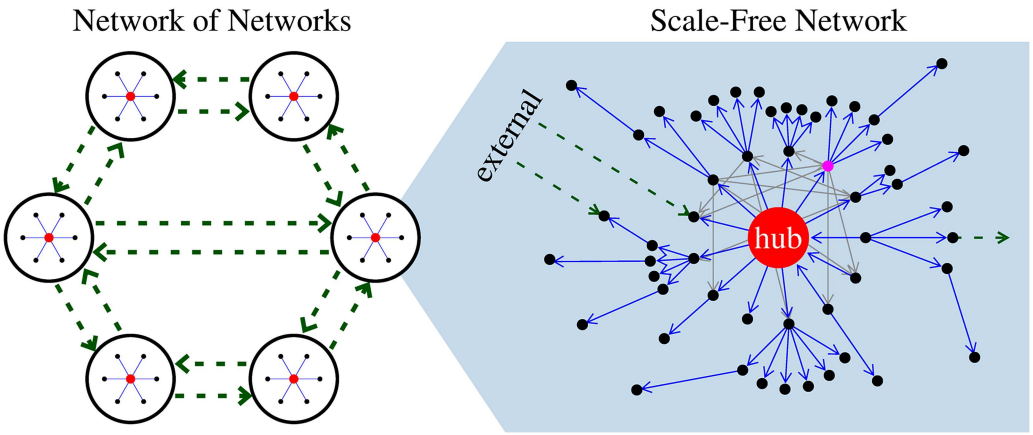

FIG. 2. Simplified scheme of the network used in numerical simulations. On the left side, we represent a network with six subnetworks (larger circumferences), although, for the study, 78 cortical regions were considered. Chemical connections (arrows dashed in green) were established between the subnetworks according to the adjacency matrix, with 50% of the connections in each direction. On the right side, we illustrate the cortical regions built with a scale-free network topology. Some connections have been omitted for greater legibility of the figure. We highlight the hub (red circle), the secondary hub (magenta circle), and the connections with other subnetworks (green dashed lines). For both schemes, each vertex represents a neuron, and all adopted connections are chemical, that is, directed (arrows in blue or gray).

the subnetworks has at least one connection in which it sends a signal and another in which it receives, respectively. Such construction prevents the existence of neurons with only outgoing or, in addition, incoming connections, which would act semi-isolated without receiving or sending signals to the network.

The chemical links are one-way,[28] so we established the coupling between the pairs of cortical regions by drawing two neurons, one in each region of the pair. The incoming and outcoming connections are defined are defined with a 50% probability in each direction. During this process, the choice of neurons is equiprobable and relevant if there is no repetition of links in both directions.[23]

Scale-free networks feature the power-law degree distribution $P(k) \propto k^{-\gamma}$, with the exponent lying between $2 \leq \gamma \leq 3$. For purposes of simplicity, in Fig. 3, we show in log × log scale the distribution obtained in only one of the subnetworks generated for the study. The power-law exponent was obtained by fitting the degree distribution ($\gamma = 2.17$), which is included in the accepted range for a scale-free network. For all subnetworks generated in this study, $\gamma \approx 2.20$. This exponent value is associated with star-like scale-free network topology, with a densely connected vertex (hub) and a few other vertices that can connect to each other.[29,30]

Once the internal and corticocortical connections are established, we obtain the adjacency matrix $\mathbb{A}$, which consists of a block matrix with 78×78 sub-matrices $\mathbb{A}_{(u,v)}$ of order 200×200. We identified the elements of $\mathbb{A}$ by the notation $a_{(u,v)(i,j)}$, where the indices u and v locate the sub-matrix of weights of the connections between the cortical regions, where i and j are the vertices of the u and v subnetworks, respectively.

Due to the unique direction of the links, the sub-matrix is not symmetrical, with the presynaptic neuron addressed in the columns and the postsynaptic neuron in the lines, that is, $a_{(u,v)(i,j)}$ is the connection weight whose signal originated from the jth neuron of the v subnetwork and destined to the ith of the u subnetwork. The sub-matrix $\mathbb{A}_{(u,u)}$ of the main diagonal corresponds to the internal links of cortical regions in scale-free topology with unit weight. The other elements $\mathbb{A}_{(u,v\neq u)}$, outside the main diagonal, establish connections between the cortical regions. In these, the weight is determined according to the human adjacency matrix.

We can say that, in general, the adjacency matrix does not depend on the mathematical model of the neuron. In Sec. III, we describe the model adopted in this study for neuronal dynamics and the mathematical formulation of coupling between neurons.

III. NEURONAL NETWORK DYNAMICS

The neuronal dynamic is characterized by the occurrence of spikes and bursts that are related to communication between

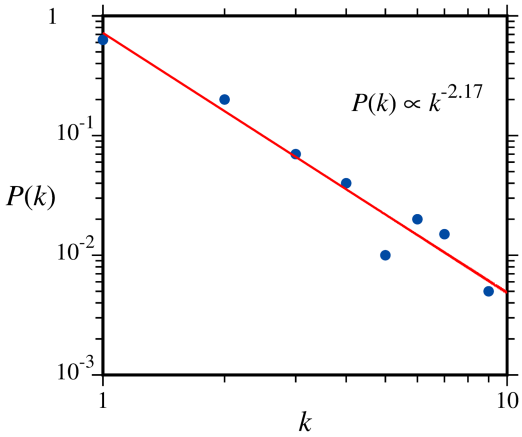

FIG. 3. Probability $P(k)$ for each degree k in a scale-free network with 200 vertices generated by the Barabási–Albert algorithm.[10] Considering a logarithmic scale, the power-law $P(k) \propto k^{-\gamma}$ is evident, being $\gamma = 2.17$.

neurons. In general, each neuron has a different neural spike rate. However, when neural spikes are combined, burst synchronization occurs causing neural firing at the same time in most neurons.

Some studies have reported neural synchronization as a cause of Parkinson's disease, essential tremors, and epilepsy.[31–33] Therefore, this research aims to find a means for suppressing neuronal synchronization using a control technique resulting from the application of perturbation as a function of the mean-field that acts on neurons.

Given this proposal, we will use the two-dimensional Rulkov's map to mimic neuronal dynamics. This map describes a phenomenological model that shows the characteristic bursts and has been widely used in recent studies about synchronization in neural networks. The Rulkov's map is written in terms of two variables: a fast (x) and a slow (y), one parameter that gives the nonlinearity to the map (α) and another that can simulate an external current (σ). The setting of the different values of these parameters gives different firing patterns.[20]

Our network structure is formed by coupling neurons according to the matrix $\mathbb{A}$ using the factor $\varepsilon\, \mathcal{C}_n^{(u,i)}$, resulting in the following equations:

$$x_{n+1}^{(u,i)} = \frac{\alpha^{(u,i)}}{1+\left[x_n^{(u,i)}\right]^2} + y_n^{(u,i)} - \varepsilon\, \mathcal{C}_n^{(u,i)}, \tag{1}$$

$$y_{n+1}^{(u,i)} = y_n^{(u,i)} - \sigma\left[x_n^{(u,i)} - \rho\right]. \tag{2}$$

The upper indexes u and i identify the cortical region and the neuron, respectively. We define the typical parameters for the Rulkov's map $\sigma = 10^{-3}$, $\rho = -1$, and $\alpha \in [4.1, 4.3)$. The choice of these values contemplates the range for which the Rulkov's map mimics the neuronal burst dynamics.[20,34]

As for the connections, ε is the chemical coupling parameter with $\varepsilon = 0$ being the case where neurons are not coupled. $\mathcal{C}_n^{(u,i)}$ carries information from synapses, specifically accumulating all signals received by the ith neuron from the uth cortical region; this includes the internal and external connections. Thus,

$$\mathcal{C}_n^{(u,i)} = \frac{1}{K^{(u,i)}} \sum_{v=1}^{N} \sum_{j=1}^{M} a_{(u,v)(i,j)} H\left(x_n^{(v,j)} - \theta\right)\left[x_n^{(u,i)} - V_{(u,v)(i,j)}\right], \tag{3}$$

where the sums are given over all connections destined to the considered neuron, with the number of subnetworks being $N = 78$ with $M = 200$ maps in each. The term $a_{(u,v)(i,j)}$ is the weight matrix that addresses the connections between different cortical regions. Here, $K^{(u,i)}$ is the number of connections directed to the neuron (u, i), and $H(\cdot)$ is the Heaviside function, defined by

$$H(q) := \begin{cases} 0, & \text{for } q < 0, \\ 1, & \text{for } q \geq 0. \end{cases} \tag{4}$$

So, if $a_{(u,v)(i,j)} \neq 0$ and $x_n^{(v,j)} > \theta$, there is signal transmission from element (v, j) to (u, i). We adopt the threshold potential $\theta = -1$. The chemical synapses may be excitatory or inhibitory, distributed in 75% (excitatory) and 25% (inhibitory).[35,36] Such distinction is given through the potential $V_{(u,v)(i,j)}$, with the condition

$$V_{(u,v)(i,j)} = \begin{cases} 1.0, & \text{(excitatory)}, \\ -0.5, & \text{(inhibitory)}. \end{cases} \tag{5}$$

Recent studies employ a similar formulation for both the coupling term[23,37,38] and the Rulkov neuron, thus being a good basis for studying the dynamic behavior of the system. It is important to mention that we consider non-identical neurons, with the diversity being promoted through a random choice of $\alpha^{(u,i)}$ values in the referred interval.

The network synchronization takes place according to parameter ε, a characteristic analyzed in Sec. IV A. Assuming $\varepsilon = 0.10$, we observe synchronized neuronal activity and, consequently, the mean-field

$$X_n^{(u)} = \frac{1}{M} \sum_{i=1}^{M} x_n^{(u,i)}, \tag{6}$$

calculated in each cortical region, it presents oscillations following the bursts. In Fig. 4(a), we superimpose the time series of $x_n^{(1,1)}$ (black line) and $X_n^{(1)}$ (red line), where we can see the biggest variations in the mean-field of the subnetwork, following the rhythm of the bursts, which start at the times labeled n_k's.

Among the methods to reduce or suppress synchronization in neuronal networks, one that has been widely used is suppression by a time-delayed feedback[39–41].Contrary to the usual technique, our approach is to use a perturbation that acts in the mean-field of

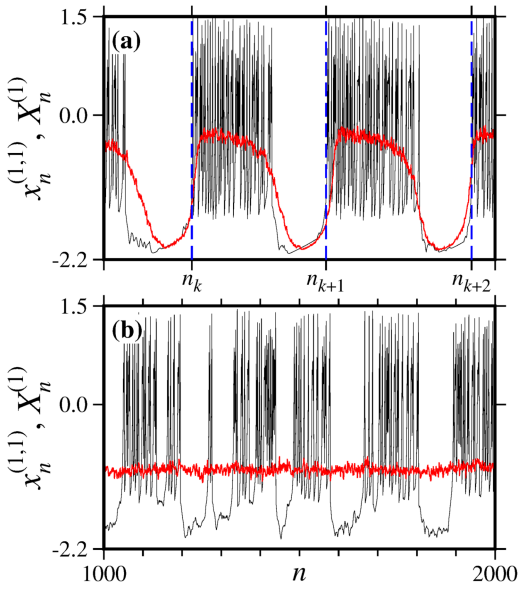

FIG. 4. Parts from the time series of the variable $x_n^{(1,1)}$ (black line) and mean-field $X_n^{(1)}$ (red line) from the same subnetwork, $\varepsilon = 0.1$ in both frames. (a) Synchronized case obtained in the absence of perturbation, oscillations in the mean-field follow the bursts. The dashed vertical lines mark the n_k's start times for bursts. (b) Non-synchronized case with $\beta = 0.028$ and $\tau = 1$ in Eq. (7); the mean-field does not follow the bursts dynamics.

the neuronal membrane potential suppressing synchronization only when necessary. The perturbation is chosen at two levels: 0 or β, which is switched by the average of the mean-field in each subnetwork. When the average of the mean-field passes a threshold (θ), the perturbation is activated. This perturbation will be added to Eq. (1) in the form

$$x_{n+1}^{(u,i)} \mapsto x_{n+1}^{(u,i)} - \beta\, H\left(X_{n,\tau}^{(u)} - \theta\right). \tag{7}$$

The presence of synchronization in the subnetwork causes a regular oscillation in its mean-field. Thus, inserting a negative term in Eq. (7), after the mean-field exceeds a given threshold, prevents this oscillatory behavior.

By adopting the average of the mean-fields calculated in the last iterations, we aim to reduce the effects of the abrupt oscillations observed during the bursts. In Eq. (7), β is the magnitude of the perturbation, τ is the accumulation time for the calculation of the mean-field measured over the previous times of the time series, and

$$X_{n,\tau}^{(u)} = \frac{1}{\tau}\sum_{k=0}^{\tau-1}\frac{1}{M}\sum_{i=1}^{M} x_{n-k}^{(u,i)} = \frac{1}{\tau}\sum_{k=0}^{\tau-1} X_{n-k}^{(u)} \tag{8}$$

is the current time average of the mean-field of the uth cortical region, note that $X_{n,\tau=1}^{(u)} = X_n^{(u)}$. The mean-field value plays an important role in the evaluation of neuronal network synchronization. If the network is synchronized, the mean-field is characterized by a large amplitude of oscillation and high variance [Fig. 4(a)]. If the network is not synchronized, the mean-field will have low amplitude and low variance.

The time series under the effect of perturbation can be seen in Fig. 4(b), with $\beta = 0.028$ and $\tau = 1$ in Eq. (7). Similar to the one shown in Figs. 4(a), in (b), the curves of subnetworks' mean-field (red line) and the neuron fast variable (black line), both from the region 1, are superimposed. The included perturbation leads to the non-synchronization of neuronal activity, which can be seen through the mean-field, since the variation in its amplitude does not follow the bursts dynamics, as shown in Fig. 4(b).

In Sec. IV B, we analyzed the suppression of synchronization according to parameters β and τ. When $X_{n,\tau}^{(u)} \geq \theta$ in Eq. (7), the perturbation is applied to the subnetwork; that is, when the average given in Eq. (8) reaches the burst threshold, all neurons in the cortical region receive the same pulse of intensity $-\beta$. In Eq. (8), the average of the mean-field in the recent τ iterations of the system aims to circumvent the effects of oscillations around the burst threshold.

IV. METHODS

A. Neuronal burst synchronization

To measure the phase synchronization of the network, we use the Kuramoto order parameter.[1,42,43] This indicator has been used successfully in recent studies, allowing to analyze phase synchronization between neuronal patterns such as spikes and bursts. In our model, we calculate the Kuramoto order parameters for the (i) network formed by the corticocortical connections and within the subnetworks (global network) and (ii) only for the subnetworks. For the first case, the global network, we define the Kuramoto order parameter as

$$\bar{R} := \frac{1}{(n_b - n_a + 1)NM}\sum_{n=n_a}^{n_b}\left|\sum_{u=1}^{N}\sum_{i=1}^{M} e^{i\varphi_n^{(u,i)}}\right|, \tag{9}$$

where the sum occurs over the $M = 200$ neurons of the $N = 78$ cortical regions. Times $n_a < n_b$ delimit the closed evaluation interval, being $(n_b - n_a + 1)$ the total iterations in that interval. The phase $\varphi_n^{(u,i)}$ associated to ith neuron of uth cortical region is given by

$$\varphi_n^{(u,i)} := 2k\pi + 2\pi\frac{n - n_k^{(u,i)}}{n_{k+1}^{(u,i)} - n_k^{(u,i)}}, \tag{10}$$

with $n_k^{(u,i)} \leq n < n_{k+1}^{(u,i)}$, where $n_k^{(u,i)}$ is the beginning of the kth burst [see Fig. 4(a)].

In addition to the evaluation of global network synchronization, the time average of the order parameter for the uth subnetwork is obtained from the following equation:

$$R^{(u)} = \frac{1}{(n_b - n_a + 1)M}\sum_{n=n_a}^{n_b}\left|\sum_{i=1}^{M} e^{i\varphi_n^{(u,i)}}\right|. \tag{11}$$

Here, Eq. (11) represents the average Kuramoto order parameter calculated for each subnetwork. In this way, the average order parameter of the subnetwork can be calculated using

$$\langle R^{(u)}\rangle = \frac{1}{N}\sum_{u=1}^{N} R^{(u)}. \tag{12}$$

Note that Eqs. (9) and (12) differ for allowing us to evaluate, separately, the synchronization of the global network and subnetworks, respectively. This evaluation is important because it shows us how synchronization occurs between different cortical regions and in different subnetworks.

The order parameter belongs to the interval $0 \leq \bar{R} \leq 1$.[42,43] When $\bar{R} = 0$, neurons are non-synchronized, and when $\bar{R} = 1$, they are said to be synchronized in phase. In general, is assumed that $\bar{R}$ values between 0 and 1 correspond to partial phase synchronization.

B. Suppression of synchronization by a function of the mean-field

Previous studies have shown success in suppressing synchronization in neural networks using a feedback technique through the mean-field.[23,37,44] We also investigate the effects of perturbation as a function of the mean-field, with the intention of suppressing synchronization. For that, we insert transformation 7 in Eq. (1), so that amplitude perturbation, $-\beta$, affects all neurons in the perturbed subnetwork since the average of the mean-fields in the last τ iterations exceeds θ.

The proposal presented in Ref. 23 uses the time-delayed feedback method as a measure of suppression through the measurement of the mean-field, with and without feedback perturbation, adjusting the intensity of the feedback control to a percentage of cortical regions. Unlike the time-delayed feedback technique, we highlight in our research, the main goal is the application of perturbation that has an effect directly on the mean-field of the network, affecting all neurons and not just a percentage of them. This perturbation

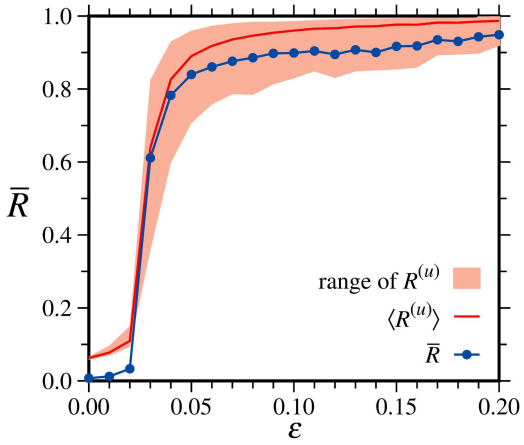

FIG. 5. Kuramoto's order parameter as a function of ε, after discarding 10^4 transient iteration and evaluating synchronization during 10^4 steps. We present the averages over 10 evolutions of the system from different initial conditions. The abscissa was discretized into 21 equidistant values in the range $\varepsilon \in [0, 0.2]$. $\bar{R}$ (blue dots) was calculated for the global network and $R^{(u)}$ (red line) is the average Kuramoto order parameter in the subnetworks, where $\langle R^{(u)} \rangle > \bar{R}$ indicates the subnetworks that are more internally synchronized than between different cortical regions.

acts in a subnetwork as a selector switch, adding or not, a perturbation depending on the value assumed by the mean-field of the fast variable of the Rulkov map, which is responsible for describing the neuron membrane potential. As we show later, the suppression method proposed in this work leads to values of $S \gg 1$ according to the relationship between the amplitude of perturbation β and coupling parameter ε.

The suppression of synchronization will be evaluated with respect to the mean-field given by Eq. (13). Several studies demonstrate the effectiveness of this type of control.[23,37,41,45] In this way, we can write

$$\zeta_n(\varepsilon, \beta, \tau) = \frac{1}{NM} \sum_{u=1}^{N} \sum_{i=1}^{M} x_n^{(u,i)}(\varepsilon, \beta, \tau), \tag{13}$$

with ε being the network coupling parameter, β being the amplitude of perturbation, and τ being the accumulation time for the calculation of the mean-field in Eq. (8), measured over the previous times of the time series. We explicit the parameter set $(\varepsilon, \beta, \tau)$ in order to map suppression according to them, as shown in Fig. 6.

As mentioned in Sec. IV A, the mean-field value plays an important role in the evaluation of neuronal network synchronization that can be seen by an analysis of mean-field variance. In this way, we will measure the suppression of the network through the mean-field variance ratio $\zeta_n(\varepsilon, \beta, \tau)$ with and without the application of the control,[41]

$$S(\varepsilon, \beta, \tau) = \sqrt{\frac{\mathrm{Var}\left[\zeta_n(\varepsilon, \beta{=}0, \tau)\right]}{\mathrm{Var}\left[\zeta_n(\varepsilon, \beta, \tau)\right]}}, \tag{14}$$

where $\mathrm{Var}[\zeta_n(\varepsilon, \beta, \tau)]$ and $\mathrm{Var}[\zeta_n(\varepsilon, \beta{=}0, \tau)]$ are the mean-field variance with and without perturbation, respectively. The success of the suppression method is achieved when $S \gg 1$. The higher the value of S, better the effect of suppression. Values of $S < 1$ imply enhanced synchronization in the disturbed region, that is, the opposite effect that we are looking for.

We highlight as an advantage of the method proposed here, in relation to others found in the literature, the possibility of implementing, in the real world, an electronic device that generates pulses of amplitude β as a function of average neuronal activity, which computed along of τ iterations within each cortical region. It is worth mentioning that high suppression is obtained with the application of the method, which significantly exceeds that obtained in previous works with similar networks.

V. RESULTS

A. Bursting synchronization

The information about network synchronization is presented in Fig. 5. For these results, we use 10^4 iterations after a 10^4 transient and a set of 10 initial conditions. It is important to say that for each new set of initial conditions, a new scale-free network is generated, respecting the same growth process and with the same number of neurons in the networks previously presented.

The average Kuramoto order parameter $\bar{R}$ for all networks is represented by the blue dotted curve in Fig. 5. Initially, the network has low synchronization for small values of ε. The synchronization value increases according to the intensity of chemical coupling. It is also possible to observe that there is an abrupt growth in synchronization for $\varepsilon = 0.02$, reaching its maximum value close to $\bar{R} \approx 0.9$.

The average Kuramoto order parameter in the 78 cortical regions, $\langle R^{(u)} \rangle$, is represented in Fig. 5 by the solid red line. We observed that the subnetworks present a greater synchronization than the composition of all networks with $\langle R^{(u)} \rangle \approx 0.99$. This includes the onset of synchronization, which, on average, presents higher values with ε very close to zero.

An indication that the subnetworks are internally more connected than the different cortical regions is the fact that the adjacent matrix of free-scale networks has unit weights, connecting all neurons within the same region; in contrast, the number of connections established between different cortical regions is given by the weight of the human connectivity matrix; for this reason, the number of internal connections (within the cortical regions) is greater than the external connections.

The maximum and minimum values of synchronization in the cortical regions can be seen by the pink region in Fig. 5. The minimum synchronization value is around $\langle R^{(u)} \rangle \approx 0.8$, while the maximum value is approximately $\langle R^{(u)} \rangle \approx 1.0$.

B. Suppression of synchronization

The results for suppression of synchronization according to parameters β and τ [Eq. (14)] are presented in Fig. 6. On the horizontal axis of the three presented frames, $\beta \in [0, 0.04]$ and is discretized in steps of 0.002. We use combinations of these parameters for $\varepsilon \in [0.05, 0.20]$, which is the interval where synchronization is observed in Fig. 5. With $\varepsilon = 0.10$, there is no suppression for $\beta \leq 0.01$ according to Figs. 6(a) and 6(b). For values of $\tau = 1, \ldots, 5$,

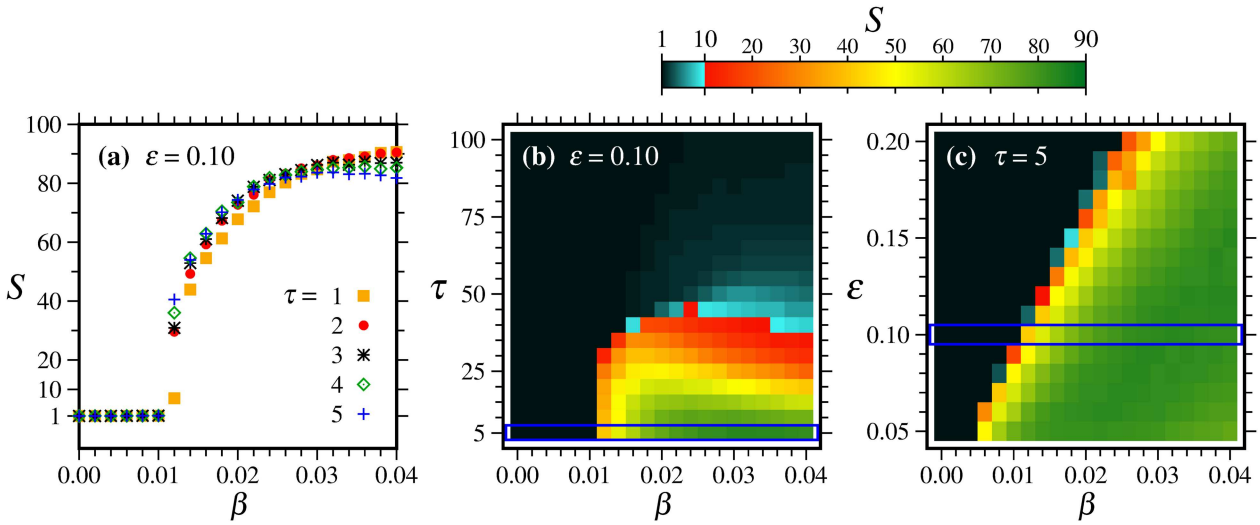

FIG. 6. Suppression of synchronization as a function of the magnitude of perturbation β for different τ. We drop a 10^4 transient, calculate S over the next 10^4 steps, and present the averages over 10 evolutions of the system from different initial conditions. In (a), we illustrate S as a function of β with τ between 1 and 5 and $\varepsilon = 0.1$. We observe the onset of suppression from $\beta = 0.012$, and the curves for different values of τ are closer to $\beta = 0.028$. (b) and (c) are the parameter space with S represented in color, according to label. In (b), $\varepsilon = 0.10$ and τ are discretized in steps of 5 units, and in (c), $\tau = 5$ and ε discretized in steps of 0.01. The blue boxes highlight equivalent regions in both figures.

the S curves as a function of β are similar, with the smallest distance between them observed in $\beta = 0.028$, from that point there is an inversion in the suppression values, which is now slightly higher for the lowest values of τ, see Fig. 6(a).

Starting from $\tau = 50$, the condition $S \gg 1$ is not obtained, as shown in Fig. 6(b), reaching modest values for suppression between $1 < S < 10$. In this case, synchronization is not significantly suppressed when compared to other cases analyzed. In Fig. 6(c), we set $\tau = 5$ and calculate S for pairs (β, ε). We observed that the suppression value also depends on the values adopted for chemical coupling parameter ε since, with higher values, we obtain higher values for suppression. The blue boxes highlight the equivalent regions in Figs. 6(b) and 6(c).

Another interesting observation is the fact that some initial conditions are shown to be more robust to perturbation, keeping neuronal activity synchronized. In Fig. 7, we show $\bar{R}$ for $\beta = 0.028$ and $\tau = 1$. The points $\bar{R}_-$ and $\bar{R}_+$ are the averages of the order parameter for cases higher or lower than 0.5, respectively. The occurrence rate of order parameter greater than 0.5 is indicated by yellow triangles, and it was observed only for $\varepsilon \geq 0.17$, from that value, the percentage of initial conditions that lead to robust states to the perturbation grows fast (triangles in yellow in Fig. 7), reaching 21% in $\varepsilon = 0.20$. It is important to say that we obtain these results considering a set of 100 distinct initial conditions.

To validate the effectiveness of the presented method, we evaluate what happens with synchronization, and with the Kuramoto average order parameter, in certain regions that we will call windows. The choice of windows' evaluation allows a better visualization than during the evolution of the system. The windows are observed within 10^4 iterations (considering the same value for the transient) for 5×10^4 steps. We evaluated the system evolution with $(\varepsilon, \beta, \tau) = (0.2, 0.027, 5)$ border region between $S \approx 1$ and $S \gg 1$ in Fig. 6(c). From the results shown in Fig. 7, we infer that the success of the suppression method may depend on the initial conditions for certain pairs of parameters (ε, β). In Fig. 8, we show two different series generated changing only the initial conditions.

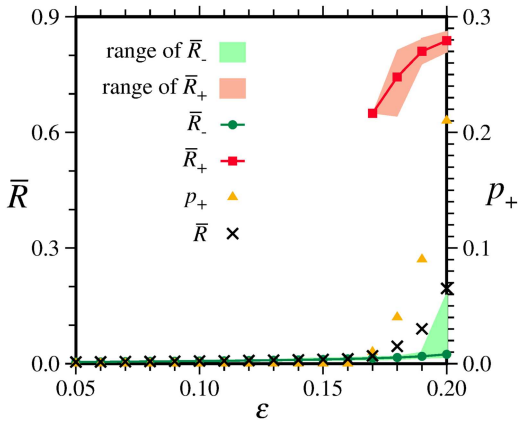

FIG. 7. Kuramoto's average order parameter obtained with $\beta = 0.028$ and $\tau = 1$. The averages are calculated for 100 different initial conditions. We highlighted $\bar{R}_+$ for the order parameter higher than 0.5 and $\bar{R}_-$ for the opposite case. We indicate p_+ as the occurrence rate of $\bar{R}_+$. The range of values observed in each case is represented in colored regions.

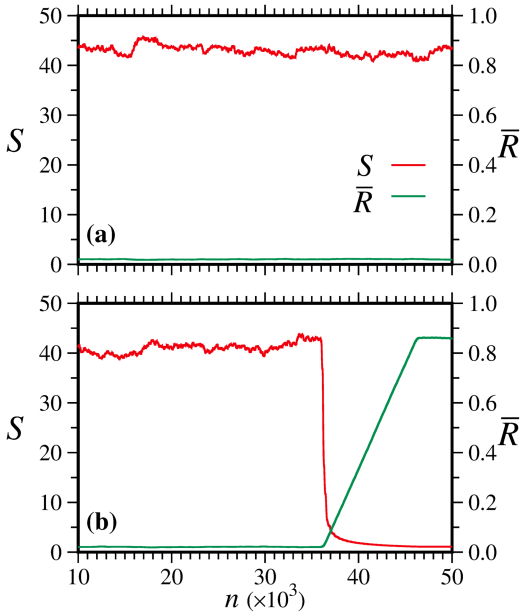

FIG. 8. Suppression S (red line) and Kuramoto average order parameter $\bar{R}$ (green line) illustrated in windows of 10^4 iterations. We can observe that when the proposed suppression method is successful, S reaches high values while $\bar{R}$ reaches low values (a). When the method stops working, S drops abruptly and $\bar{R}$ grows rapidly until it reaches values close to the unit (b).

In Fig. 8(a), we show a case for which synchronization is suppressed by more than 5 times the number of iterations evaluated in the frames in Fig. 6, that is, by 5×10^4 iterations in addition to 10^4 evaluated previously. This can be seen by the high value of S, with maximum values reaching approximately $S \approx 43$, with small fluctuations. On the other hand, in Fig. 8(b), we find a case in which the suppression method stops working and leads to a synchronization of the network after a certain number of iterations. As we can see, initially, the suppression values are high (as opposed to the synchronization values), and after 36×10^3 iterations, the situation is reversed, causing S to fall to values close to 1 and $\bar{R}$ increase, reaching values above 0.8. This indicates that, for the case of Fig. 8(b), the perturbation method by the addition of a $-\beta$ factor works well to suppress the synchronization of the network for a certain number of iterations. After that, the perturbation ceases to have the effect and the network starts to synchronize, causing an increase in the order parameter until it stabilizes. Considering that we calculate $\bar{R}$ in the window of the last 10^4 iterations, the ramp-up seen in Fig. 8(b) is related to an abrupt synchronization that occurred after 36×10^3 iterations; this sudden synchronization is clear on the curve for S, which falls rapidly from $S = 40$ to approximately $S = 1$.

In order to extend the suppression of synchronization to longer times, we modified the perturbation as a function of variance of $x_n^{(u,i)}$ in each subnetwork. Given that we observed an abrupt synchronization for pairs (ε, β) in the border region between $S \gg 1$ and $S \approx 1$ in Fig. 6(c), we propose to increase the amplitude of perturbation by taking the pair (ε, β) to regions where the synchronization was not observed in the evaluated time interval, and now, we will have the perturbation applied at three levels: $0, \beta < 0.04$, or $\beta = 0.04$. Being

$$\beta \mapsto 0.04, \quad \text{if Var}\left(x_n^{(u,i)}\right)_i < 1. \tag{15}$$

That is, we use $\beta = 0.04$ for networks where the variance of the fast variable is less than the unit in the previous iteration, keeping the value of the perturbation parameter unchanged when $\text{Var}(x_n^{(u,i)})_i \geq 1$. Again, the perturbation is activated when the mean-field exceeds θ. The selection of β level less than 0.04 or equal to 0.04 depends on the variance of the variable $x_n^{(u,i)}$ in the previous iteration in each subnetwork.

We performed tests with modified perturbation for $(\varepsilon, \beta, \tau) = (0.2, 0.027, 5)$ starting from 100 different initial conditions, discarding the first 10^4 iterations and calculating S and $\bar{R}$ in windows of 10^4 steps over 5×10^4 iterations. For all cases, we obtained $S \gg 1$ and, equivalently, $\bar{R} \approx 0$, with the proposed modification being a successful alternative to extend the suppression of synchronization to longer times. We also computed the number of times that the perturbation was applied to each subnetwork during 100 repetitions, being applied on average to 51% of the iterations with 22% of these triggered the change $\beta = 0.04$. In Fig. 9, we compare the cases without change in perturbation [Fig. 9(a)] with the result of the change in β [Fig. 9(b)], both started with the same initial condition. The upper frame is an extension of that shown in Fig. 8(b), where the network abruptly synchronizes after approximately 36×10^3 iterations after the transient. In the bottom frame, with the modified perturbation acting, the network does not present synchronization in the

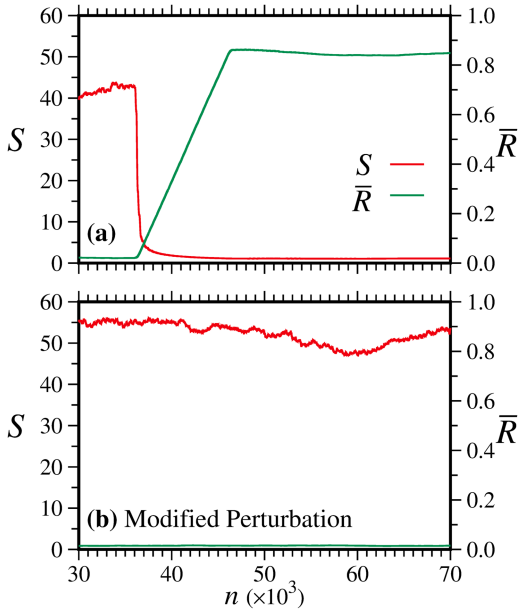

FIG. 9. Comparison between cases without (a) and with (b) perturbation β, both evolving from the same initial condition. Suppression S (red line) and Kuramoto average order parameter $\bar{R}$ (green line) are illustrated in windows of 10^4 iterations. We note that the change in β leads to higher values of S, with $\bar{R}$ very close to 0, while keeping the network out of synchronization.

evaluated time interval, as well as higher values of S and $\bar{R}$ are very close to 0.

VI. DISCUSSIONS

The evaluation of synchronization revealed that when the network is composed as a model with internal and external connections, there is, initially, very low synchronization resulting in values of $\bar{R}$ close to zero. From a threshold of network chemical coupling, there is a significant change in the dynamics of the system: the network synchronizes itself abruptly, quickly reaching values greater than $\bar{R} = 0.6$, which indicates high phase synchronization. The same phenomenon was observed when evaluating synchronization for each subnetwork. All of them, after a chemical coupling threshold, exhibit the same behavior observed in the global network (composed of internal + external connections).

An interesting situation was observed when comparing these two measures, we found that the synchronization of subnetworks is greater than that of the global network. This is because the subnetworks are internally more connected than the cortical regions (external connections made by the human connectivity matrix); even though the connections' matrix of Barabási–Albert networks has unit weights, these connections are established for all neurons within the network.

The synchronization can also be evaluated through the mean-field of the network since for a synchronized network, the mean-field follows the bursts with large amplitudes. Since we aim to suppress (or reduce) burst synchronization, we add a perturbation $-\beta$ that is a function of the mean-field of the network's time series. This term acts like a selector switch; that is, it receives the values $-\beta$ or 0 if synchronization exceeds a threshold. As result, we obtained significant values for suppression, which is measured by the ratio of the mean-field with and without perturbation, which showed that the chosen control method was well employed for several values of τ considered.

Through a parameter space of $(\varepsilon, \beta, \tau)$, we saw that when we consider ε to be fixed, the suppression reaches high values of $S > 50$ for certain combinations of β and τ, reaching values lower than $S < 10$, for longer times $\tau > 40$. When we evaluate the suppression factor with fixed $\tau = 5$ (where we had the highest suppression values), we see a large of the plan $(\varepsilon, \beta, \tau)$ where $S > 10$, which indicates a good use of the implemented method. We also found that some initial conditions seem to be more robust to the perturbation factor, keeping the system synchronized.

We also evaluate the Kuramoto order parameter and suppression in windows of 10^4 steps and show that, in fact, different initial conditions lead to different cases for S and $\bar{R}$. In the same way that the evaluation of synchronization was considered, the suppression also falls abruptly and, on the other hand, synchronization grows in the same way, which characterizes two situations in which we can validate the success of the adopted method. We also show that a slight change in the perturbation in each subnetwork $(x_n^{(u,i)})$ extends, in time, the suppression of synchronization for cases where an abrupt synchronization was observed, thus extending the success of the proposed method for certain regions of $\varepsilon \times \beta$ plan.

Although there is a similarity to the work already published in Ref. 23, when we evaluate the Kuramoto average order parameter to measure synchronization (as this is a characteristic of the network model studied according to the value of parameters adopted in this research), the results achieved for the suppression of synchronization are quite different. As we could see, our results show that the suppression of synchronization reaches values $S \gg 1$ for the majority of the presented cases, in contrast with Ref. 23, wherewith the control technique of the time-delayed feedback showed some regions of parameter space where the method was successful but reaching suppression values close to $S \approx 3.30$. It is important to make clear that this does not invalidate the use of the time-delayed feedback control method because, as it is known, this method is well applied for other systems. We also emphasize that the method to suppress synchronization proposed in this research allows us to evaluate some specific windows where there is high synchronization and to "turn on" the control to suppress synchronization in the evaluated region, which contrasts with the result obtained in the Ref. 23 in which by increasing the percentage of cortical regions in which the time-delayed feedback was applied, there was an increase in synchronization. Even when considering the topology of the Barabási–Albert networks, when the feedback control was applied in the hubs, there was no significant effect on suppression. And yet, when considering 100% of the network, the results for the suppression factor were always less than those achieved by applying perturbation in the mean-field.

VII. CONCLUSIONS

In this article, we analyzed the burst phase synchronization in a neuronal network whose connection architecture is set in levels by internal links that connect neurons within scale-free subnetworks and the connections performed between distinct cortical regions (corticocortical) through a human connectivity matrix. We seek to suppress the synchronization of neuronal bursts, given the neurological interest in this issue. Our model uses a method based on feedback with the increment of a selector switch that applies the control only for the necessary time to suppress the network synchronization.

Our results showed the advantage of using the feedback method by including the selector switch instead of the usual time-delayed feedback method. The suppression of synchronization was achieved, reaching values of $S \gg 1$ for the majority combinations of the considered parameters. Also, we show that after the perturbation stops, we can keep low network synchronization after a long time, making this method a good tool to reduce or almost completely suppress synchronization in systems of coupled networks. Although our model considers an idealized situation, applying the perturbation in the whole network is relevant to allow us to understand how this method can help to improve this study for different sets and network constructions.

ACKNOWLEDGMENTS

This study was possible by partial financial support from the following agencies: Brazilian National Council for Scientific and Technological Development (CNPq) Process Nos. 161949/2020-7, 407299/2018-1, 302665/2017-0, and 420699/2018-0. Coordination for the Improvement of Higher Education Personnel

(CAPES), and São Paulo Research Foundation (FAPESP) Process No. 2018/03211-6.

DATA AVAILABILITY

The data that support the findings of this study are available from the corresponding author upon reasonable request.

REFERENCES

[1]S. H. Strogatz, "Exploring complex networks," Nature **410**, 268–276 (2001).
[2]M. E. J. Newman, "The structure and function of complex networks," SIAM Rev. **45**, 167-256 (2003).
[3]S. A. Kauffman, "Metabolic stability and epigenesis in randomly constructed genetic nets," J. Theor. Biol. **22**, 437–467 (1969).
[4]D. S. Bassett and O. Sporns, "Network neuroscience," Nat. Neurosci. **20**, 353-364 (2017).
[5]G. Wainrib and J. Touboul, "Topological and dynamical complexity of random neural networks," Phys. Rev. Lett. **110**, 118101 (2013).
[6]D. S. Bassett and E. Bullmore, "Small-world brain networks," Neuroscientist. **12**, 512–523 (2006).
[7]J. I. Perotti, F. A. Tamarit, and S. A. Cannas, "A scale-free neural network for modelling neurogenesis," Physica A **371**, 71–75 (2006).
[8]G. L. Pellegrini, L. Arcangelis, H. J. Herrmann, and C. Perrone-Capano, "Activity-dependent neural network model on scale-free networks," Phys. Rev. E **76**, 016017 (2007).
[9]A. D. Broido and A. Clauset A, "Scale-free networks are rare," Nat. Commun. **10**, 1017 (2019).
[10]A.-L. Barabási and R. Albert, "Emergence of scaling in random networks," Science **286**, 509–512 (1999).
[11]V. M. Eguíluz, D. R. Chialvo, G. A. Cecchi, M. Baliki, and A. V. Apkarian, "Scale-free brain functional networks," Phys. Rev. Lett. **94**, 018102 (2005).
[12]E. L. Lameu, C. A. S. Batista, A. M. Batista, K. C. Iarosz, R. L. Viana, S. R. Lopes, and J. Kurths, "Suppression of bursting synchronisation in clustered scale-free (rich-club) neuronal networks," Chaos **22**, 043149 (2012).
[13]G. Deco, A. Buehlmann, T. Masquelier, and E. Hugues, "The role of rhythmic neural synchronization in rest and task conditions," Front. Hum. Neurosci. **5**, 4 (2011).
[14]M. Steriade, D. A. McCormick, and J. Sejnowski, "Thalamocortical oscillations in the sleeping and aroused brain," Science **262**, 5134 (1993).
[15]U. Knoblich, L. Huang, H. Zeng, and L. Li, "Neuronal cell-subtype specificity of neural synchronization in mouse primary visual cortex," Nat. Commun. **10**, 2533 (2019).
[16]P. J. Uhlhaas and W. Singer, "Neural synchrony in brain disorders: Relevance for cognitive dysfunctions and pathophysiology," Neuron **52**, 155–168 (2006).
[17]K. Lehnertz, S. Bialonski, M.-T. Hortmann, D. Krug, A. Rothkegel, M. Staniek, and T. Wagner, "Synchronization phenomena in human epileptic brain networks," J. Neurosci. Methods **183**, 42–48 (2009).
[18]C. Park, R. M. Worth, and L. L. Rubchinsky, "Fine temporal structure of beta oscillations synchronization in subthalamic nucleus in Parkinson's disease," J. Neurophysiol. **103**, 2707–2716 (2010).
[19]C.-Y. Lo, P.-N. Wang, K.-H. Chou, J. Wang, Y. He, and C.-P. Lin, "Diffusion tensor tractography reveals abnormal topological organization in structural cortical networks in Alzheimer's disease," J. Neurosci. **30**, 16876–16885 (2010).
[20]N. F. Rulkov, "Regularization of synchronized chaotic bursts," Phys. Rev. Lett. **86**, 183 (2001).
[21]E. L. Lameu, S. Yanchuk, E. E. N. Macau, F. S. Borges, K. C. Iarosz, I. L. Caldas, P. R. Protachevicz, R. R. Borges, R. L. Viana, J. D. Szezech, A. M. Batista, and J. Kurths, "Recurrence quantification analysis for the identification of burst phase synchronisation," Chaos **28**, 085701 (2018).
[22]J. A. P. Silveira, P. R. Protachevicz, R. L. Viana, and A. M. Batista, "Effects of burst-timing-dependent plasticity on synchronous behaviour in neuronal network," Neurocomputing **436**, 126–135 (2021).
[23]A. S. Reis, K. C. Iarosz, F. A. S. Ferrari, I. L. Caldas, A. M. Batista, and R. L. Viana, "Bursting synchronization in neuronal assemblies of scale-free networks," Chaos, Solitons Fractals **142**, 110395 (2021).
[24]M. S. A. Graziano, C. S. R. Taylor, T. Moore, and D. F. Cooke, "The cortical control of movement revisited," Neuron **36**, 349–362 (2002).
[25]A. Pasupathy and E. K. Miller, "Different time courses of learning-related activity in the prefrontal cortex and striatum," Nature **433**, 873–876 (2005).
[26]B. Zingg, H. Hintiryan, L. Gou, M. Y. Song, M. Bay, M. S. Bienkowski, N. N. Foster, S. Yamashita, I. Bowman, A. W. Toga, and H.-W. Dong, "Neural networks of the mouse neocortex," Cell **156**, 1096–1111 (2014).
[27]A.-L. Barabási, *Linked: How Everything Is Connected to Everything Else and What It Means* (Plume, 2003), ISBN:0452284392.
[28]J. B. Angevine, *Encyclopedia of the Human Brain* (Academic Press, New York, 2002), pp. 313–371, ISBN:978-0-12-227210-3.
[29]D. Tsiotas, "Detecting differences in the topology of scale-free networks grown under time-dynamic topological fitness," Sci. Rep. **10**, 010630 (2020).
[30]X. F. Wang and G. Chen, "Complex networks: Small-world, scale-free and beyond," Circuits Syst. Magaz. **3**, 6–20 (2003).
[31]P. Jiruska, M. de Curtis, J. G. Jefferys, C. A. Schevon, S. J. Schiff, and K. Schindler, "Synchronization and desynchronization in epilepsy: Controversies and hypotheses," J Physiol. **591**(4), 787–797 (2013).
[32]C. Hammond, H. Bergman, and P. Brown, "Pathological synchronization in Parkinson's disease: Networks, models and treatments," Trends. Neurosci. **30**, 357–364 (2007).
[33]A. Schnitzler, C. Munks, M. Butz, L. Timmermann, and J. Gross, "Synchronized brain network associated with essential tremor as revealed by magnetoencephalography," Mov. Disord. **24**, 1629–1635 (2009).
[34]J. C. A. de Pontes, R. L. Viana, S. R. Lopes, C. A. S. Batista, and A. M. Batista, "Bursting synchronization in non-locally coupled networks," Physica A **387**, 4417–4428 (2008).
[35]T. W. Lee, *Network Balance and Its Relevance to Affective Disorders: Dialetic Neuroscience* (Pronoun, 2016), Vol. 268.
[36]C. R. Noback, N. L. Strominger, R. J. Demarest, and D. A. Ruggiero, *The Human Nervous System: Structure and Function*, 7th ed. (Humana Press, 2005).
[37]F. A. S. Ferrari, R. L. Viana, A. S. Reis, K. C. Iarosz, I. L. Caldas, and A. M. Batista, "A network of networks model to study phase synchronization using structural connection matrix of human brain," Physica A: Stat. Mech. Appl. **496**, 162–170 (2018).
[38]E. L. Lameu, F. S. Borges, R. R. Borges, K. C. Iarosz, I. L. Caldas, A. M. Batista, R. L. Viana, and J. Kurths, "Suppression of phase synchronisation in network based on cat's brain," Chaos **26**, 043107 (2016).
[39]K. Pyragas, "Delayed feedback control of chaos," Phil. Trans. R. Soc. A **364**, 2309–2334 (2006).
[40]M. G. Rosenblum and A. Pikovsky, "Delayed feedback control of collective synchrony: An approach to suppression of pathological brain rhythms," Phys. Rev. E **70**, 041904 (2004).
[41]M. G. Rosenblum and A. Pikovsky, "Controlling synchronization in an ensemble of globally coupled oscillators," Phys. Rev. Lett. **92**, 102–114 (2004).
[42]Y. Kuramoto, *Chemical Oscillations, Waves, and Turbulence*, 8th ed. (Springer-Verlag, 1984), p. 156.
[43]A. Arenas, A. Díaz-Guilera, J. Kurths, Y. Moreno, and C. Zhou, "Synchronization in complex networks," Phys. Rep. **469**, 93–153 (2008).
[44]C. A. S. Batista, A. M. Batista, J. C. A. Pontes, S. R. Lopes, and R. L. Viana, "Bursting synchronization in scale-free networks," Chaos, Solitons Fractals **41**, 2220–2225 (2009).
[45]C. A. S. Batista, S. R. Lopes, R. L. Viana, and A. M. Batista, "Delayed feedback control of bursting synchronization in a scale-free network," Neural Netw. **23**, 114–124 (2010).